Selective Methylation of Histone H3 Variant H3.1 Regulates Heterochromatin Replication

Yannick Jacob *et al.*

Science **343**, 1249 (2014);
DOI: 10.1126/science.1248357

Selective Methylation of Histone H3 Variant H3.1 Regulates Heterochromatin Replication

Yannick Jacob,[1]* Elisa Bergamin,[2]* Mark T. A. Donoghue,[1] Vanessa Mongeon,[2] Chantal LeBlanc,[1] Philipp Voigt,[3] Charles J. Underwood,[1] Joseph S. Brunzelle,[4] Scott D. Michaels,[5] Danny Reinberg,[3] Jean-François Couture,[2]† Robert A. Martienssen[1,6]†

Histone variants have been proposed to act as determinants for posttranslational modifications with widespread regulatory functions. We identify a histone-modifying enzyme that selectively methylates the replication-dependent histone H3 variant H3.1. The crystal structure of the SET domain of the histone H3 lysine-27 (H3K27) methyltransferase *ARABIDOPSIS* TRITHORAX-RELATED PROTEIN 5 (ATXR5) in complex with a H3.1 peptide shows that ATXR5 contains a bipartite catalytic domain that specifically "reads" alanine-31 of H3.1. Variation at position 31 between H3.1 and replication-independent H3.3 is conserved in plants and animals, and threonine-31 in H3.3 is responsible for inhibiting the activity of ATXR5 and its paralog, ATXR6. Our results suggest a simple model for the mitotic inheritance of the heterochromatic mark H3K27me1 and the protection of H3.3-enriched genes against heterochromatization during DNA replication.

During the S phase of the cell cycle, patterns of histone posttranslational modifications (PTMs) must be reestablished after passage of the replication fork to restore the correct epigenetic status to each region of the genome (*1*). Because many different chromatin states are encountered during replication, the deposition of histone PTMs on newly replicated chromatin must be precisely regulated.

The histone H3 Lys^{27} (H3K27) methyltransferases *ARABIDOPSIS* TRITHORAX-RELATED PROTEIN 5 (ATXR5) and ATXR6 (ATXR5/6) are thought to maintain the heterochromatic mark H3K27me1 during DNA replication in plants (*2*). In *atxr5 atxr6* double mutants, H3K27me1 levels are reduced, heterochromatin is decondensed, some repetitive sequences are transcribed, and heterochromatic overreplication is observed (*3*–*5*). In both animals and plants, chromatin restoration after DNA replication depends on the histone chaperone CAF-1 and involves deposition of the S-phase–expressed histone H3 variant H3.1 (*6*, *7*). In contrast, histone H3.3 is inserted by other histone chaperones, mainly during transcription, and acts as a replacement histone (*7*–*11*). Canonical histone H3.1 and histone H3.3 are >96% identical in most eukaryotes (*12*) and differ only by four and five residues in flowering plants and mammals, respectively (Fig. 1A). H3.1 and H3.3 variants have been shown to contain different histone PTMs, but the mechanisms involved in H3 variant–specific marking are not known (*12*). It is possible that sequence variation between the variants could directly affect their PTMs (*13*, *14*).

One of the conserved differences between H3.1 and H3.3 is at position 31, with alanine (H3.1), threonine (H3.3 *Arabidopsis*), or serine (H3.3 human) (Fig. 1A). Because residue 31 of histone H3 is close to the modifiable and functionally important residue K27 (Lys^{27}), we hypothesized that H3 variants could selectively regulate methylation at K27. To test this, we performed histone lysine methyltransferase (HKM) assays using methyltransferases from *Arabidopsis thaliana* and recombinant chromatin containing either plant histone H3.1 or plant histone H3.3. Our results show that the H3K27 methyltransferases ATXR5/6 have much higher activity on nucleosomes containing H3.1 than H3.3 (Fig. 1B). Furthermore, steady-state kinetic analysis of ATXR5 confirms that the enzyme exhibits strong preference toward the H3.1 variant (Fig. 1C). This ability to favor H3.1 nucleosomes over H3.3 nucleosomes as substrates was not observed for two polycomb repressive complex 2 (PRC2) complexes [MEDEA (MEA) and CURLY LEAF (CLF)], which also methylate K27, or the H3K9 methyltransferases KRYPTONITE (KYP)/SU(VAR)3-9 HOMOLOG 4 (SUVH4) and SUVH5 (Fig. 1B). We tested whether Ala^{31} of H3.1 is required for H3K27 methylation by ATXR5/6. When using H3.3 nucleosomes with Thr^{31} replaced with alanine (T31A), we observed levels of H3K27 methylation similar to levels obtained when H3.1 nucleosomes are used (Fig. 1D). Taken together, these results demonstrate that ATXR5/6 selectively methylate the replication-dependent variant H3.1 in vitro and that Thr^{31} in H3.3 is responsible for inhibiting the activity of ATXR5/6.

To gain a better understanding of how ATXR5/6 specifically methylate H3.1, we solved the crystal structure of an ATXR5-H3.1 complex. We focused on the C-terminal half of ATXR5, which contains the catalytic SET domain preceded by a conserved sequence (hereafter named nSET) of unknown function (fig. S1). The structure of the ATXR5 homolog from the plant *Ricinus communis* [RcATXR5 amino acids 158 to 374] in complex with a histone H3.1 peptide (amino acids 18 to 36, strictly conserved between *A. thaliana* and *R. communis*) and the product cofactor S-adenosylhomocysteine (AdoHcy) was solved at 2.1 Å resolution (fig. S2 and table S1). Collectively, the structure shows that the SET domain comprises two short α helices (α5 and α6) and 10 β strands (β1 to β10), all forming twisted antiparallel β sheets (Fig. 2A). The nSET region folds as four consecutive α helices (α1 to α4) interspersed by loops that pack onto the SET domain. The H3.1 peptide binds in a tight binding cleft in an L-shaped conformation and engages in several hydrogen bonds and hydrophobic contacts (see supplementary text) with RcATXR5 (Fig. 2, A and B). A simulated annealing $F_o - F_c$ omit map revealed electron density for residues 24 to 36 of histone H3.1 (Fig. 2C). A comparative analysis of the ATXR5/H3.1 complex reveals structural divergence in the histone-binding mode (fig. S3 and supplementary text).

The ternary structure shows that both SET and nSET of RcATXR5 are involved in selective H3.1 binding. The residues E212 and M216 (E, Glu; M, Met) of the α3-α4 loop (L1) of nSET, along with R334 (R, Arg) in the SET domain, form a shallow binding pocket (referred to as selectivity pocket) accommodating the small side chain of H3.1 Ala^{31} (Fig. 3A). Accordingly, E212, M216, and R334 are strictly conserved in ATXR5/6 homologs from mosses to flowering plants (fig. S1). The side chain of Ala^{31} makes hydrophobic and van der Waals contacts with the side chains of M216 and R334, and the guanidium group of R334 engages in two short hydrogen bonds with the carboxylate group of E212, which likely rigidify the specificity pocket. Consistent with our HKM assays (Fig. 1D), we found that replacing Ala^{31} with Thr^{31} generates van der Waals clashes between the Thr^{31} Cγ methyl group and the side chain of R334 (fig. S4). In addition, amino acid substitutions at E212 and R334 (*A. thaliana* ATXR6 residues E186 and R309) drastically reduced methylation on nucleosomes (Fig. 3B), suggesting that residues forming the specificity pocket are important for conferring specificity and high affinity binding to H3.1.

Another unique structural feature of ATXR5/6 likely contributes to the selective methylation of histone H3.1. A loop (L3) comprising residues G363, Y364 (Y, Tyr), E365, and E367 folds back on top of H3.1, shielding the peptide from the solvent in a "safety belt" conformation (Figs. 2, A and B, and 3A). Y364 makes hydrophobic

[1]Howard Hughes Medical Institute–Gordon and Betty Moore Foundation, Watson School of Biological Sciences, Cold Spring Harbor Laboratory, 1 Bungtown Road, Cold Spring Harbor, NY 11724, USA. [2]Ottawa Institute of Systems Biology, Department of Biochemistry, Microbiology and Immunology, University of Ottawa, Ottawa, Ontario K1H 8M5, Canada. [3]Howard Hughes Medical Institute, Department of Biochemistry and Molecular Pharmacology, New York University School of Medicine, New York, NY 10016, USA. [4]Feinberg School of Medicine, Department of Molecular Pharmacology and Biological Chemistry, Northwestern University, Chicago, IL 60611, USA. [5]Department of Biology, Indiana University, 915 East Third Street, Bloomington, IN 47405, USA. [6]Institut de Biologie de l'École Normale Supérieure, 75005 Paris, France.

*These authors contributed equally to this work.
†Corresponding author. E-mail: jean-francois.couture@uottawa.ca (J.F.C.); martiens@cshl.edu (R.A.M.)

contact with Pro[30], while the carboxylate group of E365 engages in hydrogen bonds with the guanidium group of Arg[26] and the hydroxyl group of T289. Together, these residues help bind the peptide tightly to the histone H3.1 binding cleft. The role of the L3 loop is likely twofold: (i) locking the peptide in a conformation that forces the side chain of Ala[31] into the specificity pocket and (ii) packing the structurally constrained residue Pro[30] onto the peptide-binding pocket of RcATXR5. This hypothesis is supported by our HKM assays showing that substitution of Y364 (*A. thaliana* ATXR6 Y339) by an alanine residue reduces the specificity of the enzymes for H3.1 by threefold (Fig. 3B).

In *Arabidopsis*, H3K27me1 is enriched on H3.1 (fig. S5) (*15*, *16*), and more than 80% of H3.1 was found to be methylated at K27 by mass spectrometry (*17*). To validate that Thr[31] in histone H3.3 directly interferes with the activity of ATXR5/6 in vivo, we generated transgenic *Arabidopsis* plants expressing the tandem histone H3.1 genes *HTR9* and *HTR13* as wild-type (WT) proteins (H3.1) or with an alanine-to-threonine replacement at position 31 (H3.1 A31T). The transgenes were expressed in H3.1 quadruple mutants (*A. thaliana* contains five H3.1 genes). We quantified by chromatin immunoprecipitation (ChIP) the levels of H3K27me1 at genomic regions enriched in H3.1 (fig. S6) and that have been shown to be dependent on ATXR5/6 for H3K27me1 (*4*), because plant PRC2 complexes also have the ability to monomethylate H3K27 (fig. S7). When we measured H3K27me1 levels in the two sets of transgenic plants, we observed lower levels of the epigenetic mark in plants expressing H3.1 A31T compared to WT (Col), but not in plants expressing H3.1 (Fig. 4A and fig. S8). As in *atxr5 atxr6* double mutants, silencing of *Athila* open reading frame 1 [also known as *transcriptionally silent information* (*TSI*)] was lost in transgenic plants expressing H3.1 A31T (Fig. 4B).

Reactivation of *TSI* and other heterochromatic defects has also been observed when the histone chaperone CAF-1 is mutated in *Arabidopsis* (Fig. 4B) (*18*–*22*). Depletion of CAF-1 in mammalian cell lines leads to H3.1 replacement with H3.3 (*23*). Consistently, *Arabidopsis* CAF-1 mutants show higher expression of H3.3 genes (*18*). On the basis of our finding that ATXR5/6 specifically methylate H3.1, we hypothesized that

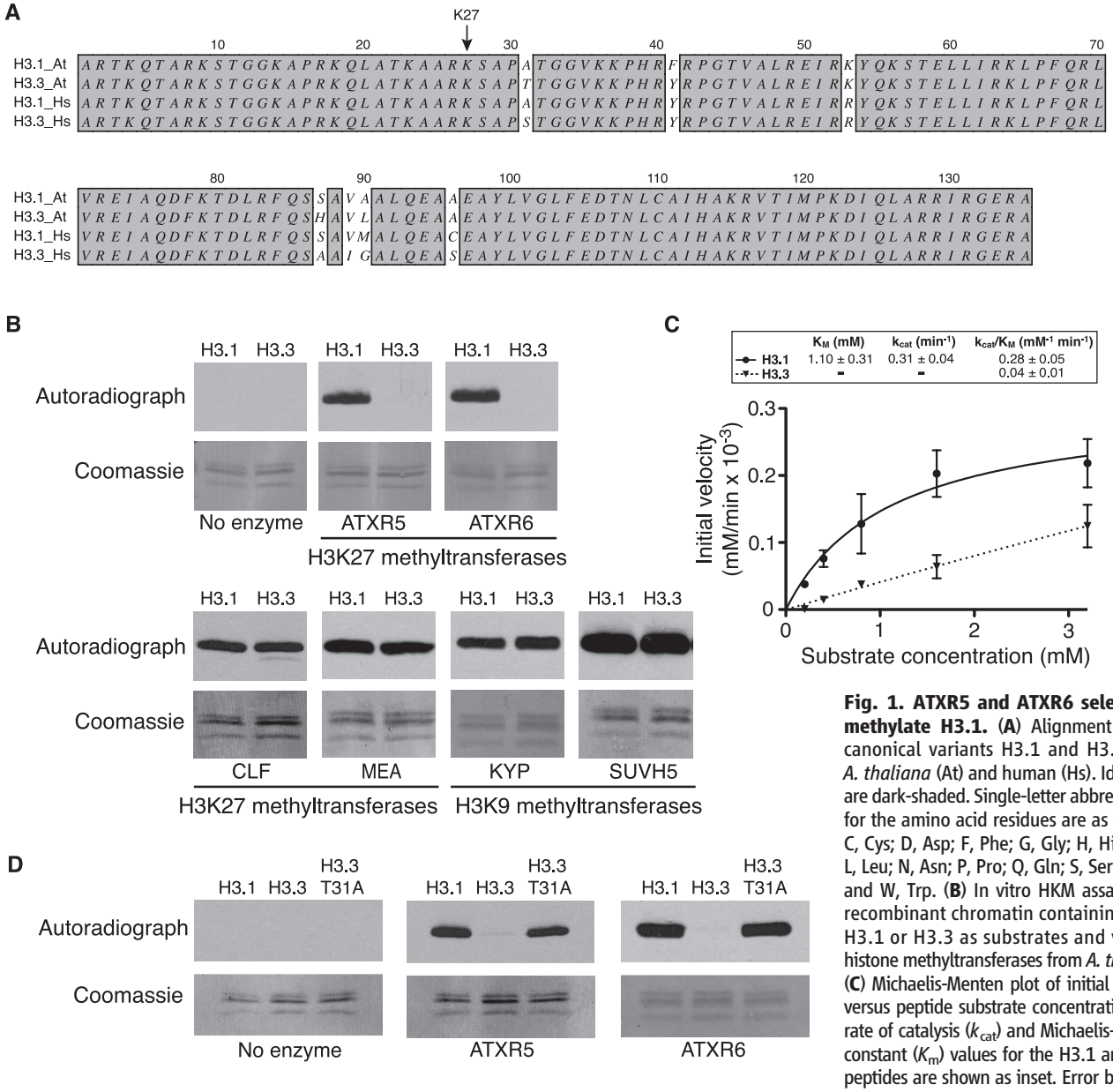

Fig. 1. ATXR5 and ATXR6 selectively methylate H3.1. (**A**) Alignment of the canonical variants H3.1 and H3.3 from *A. thaliana* (At) and human (Hs). Identities are dark-shaded. Single-letter abbreviations for the amino acid residues are as follows: C, Cys; D, Asp; F, Phe; G, Gly; H, His; I, Ile; L, Leu; N, Asn; P, Pro; Q, Gln; S, Ser; V, Val; and W, Trp. (**B**) In vitro HKM assay using recombinant chromatin containing plant H3.1 or H3.3 as substrates and various histone methyltransferases from *A. thaliana*. (**C**) Michaelis-Menten plot of initial velocity versus peptide substrate concentration. The rate of catalysis (k_{cat}) and Michaelis-Menten constant (K_m) values for the H3.1 and H3.3 peptides are shown as inset. Error bars represent the standard deviations of three independent experiments, each performed in triplicates with three different batches of RcATXR5. (**D**) In vitro HKM assays using recombinant chromatin containing plant H3.1, H3.3, or H3.3 T31A.

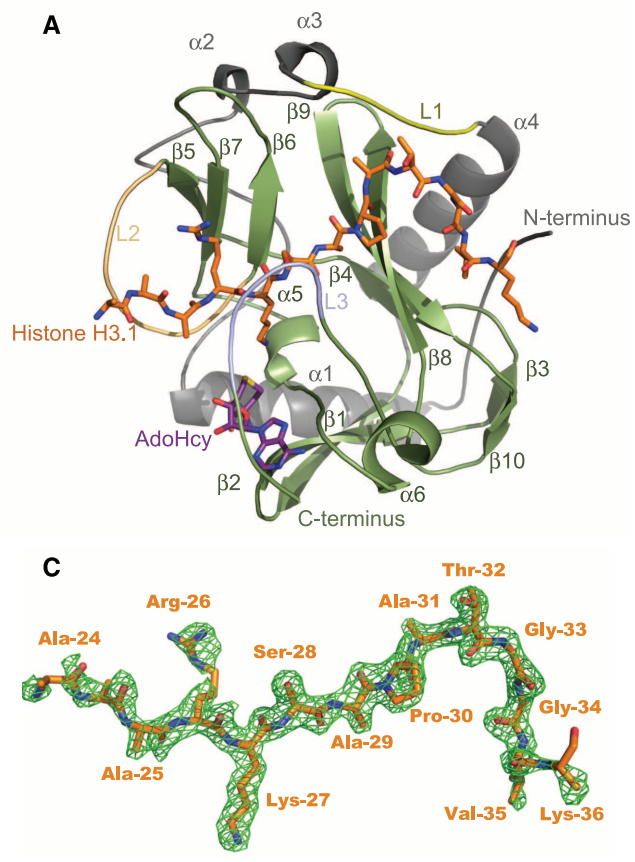

Fig. 2. ATXR5/6 contain a bipartite catalytic domain composed of nSET and SET. (**A**) Ribbon representation of the RcATXR5-H3.1-AdoHcy ternary complex in which nSET and SET are highlighted in gray and green, respectively. Carbon atoms of H3.1 and product cofactor are colored in orange and magenta, respectively. (**B**) Zoomed view of the peptide binding cleft of RcATXR5. Three-letter code refers to H3.1 residues. Carbon atoms of residues found in the L1, L2, and L3 loops are rendered in yellow, beige, and purple, respectively. The carbon atoms of other residues interacting with H3.1 are highlighted in green. Carbon atoms of H3.1 residues are colored in orange, whereas oxygen and nitrogen atoms are highlighted in red and blue. Hydrogen bonds and water molecules are illustrated as red dashed lines and red spheres, respectively. (**C**) Simulated annealing $F_o - F_c$ omit map (green) contoured at 2σ. The H3.1 peptide is rendered as in (A).

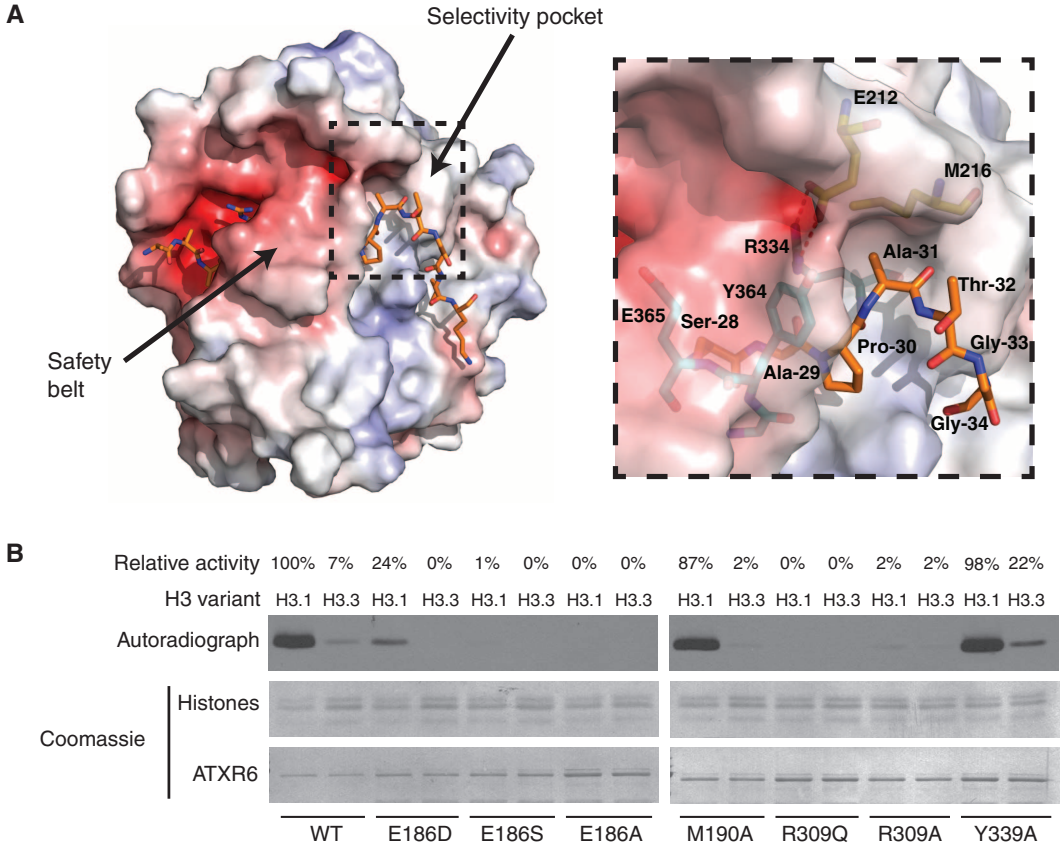

Fig. 3. The selectivity pocket and safety belt of ATXR5/6-type H3K27 methyltransferases are responsible for H3.1 preference over H3.3. (**A**) The structure of the ATXR5-H3.1-SAH complex in electrostatic potential surface representation, with the selectivity pocket and safety belt highlighted. Positive and negative potentials are in blue and red, respectively. Inlet figure shows a zoomed view of the residues forming the surface of the selectivity pocket (three-letter code refers to histone H3.1 residues). Hydrogen bonds are shown as dashed red lines. (**B**) In vitro HKM assay using recombinant chromatin containing plant H3.1 or H3.3 as substrates and WT or point mutants of ATXR6 from *A. thaliana*. The enzymatic activity indicated for each reaction is relative to the activity of ATXR6 (WT) on H3.1 nucleosomes.

the heterochromatic defects of CAF-1 mutants in *Arabidopsis* could be due, at least in part, to depletion of K27me1 when H3.3 replaces H3.1. Our results show that H3K27me1 levels are indeed lower in *fasciata2* (*fas2* encodes a subunit of CAF-1) mutants compared with Col, and this is not caused by defects in nucleosome density or antibody preference for H3.1K27me1 over H3.3K27me1 (figs. S9 and S10).

One of the phenotypes associated with reduced levels of H3K27me1 in *atxr5 atxr6* double mutants is overreplication of heterochromatic DNA (*4*). Lower levels of H3K27me1 in *fas2* mutants or our transgenic lines expressing H3.1 A31T is not accompanied by a similar defect in heterochromatic DNA replication (Fig. 4C and figs. S11 and S12) (*19*, *24*–*26*). This suggests a model in which unmethylated H3 having alanine at position 31 (i.e., H3.1K27me0) allows for heterochromatic overreplication to occur. One prediction from this model is that heterochromatic overreplication should be suppressed in a *fas2* mutant background, because H3.1K27me0 would now be replaced by H3.3K27me0. As predicted, the phenotype is strongly suppressed in *atxr5 atxr6 fas2* triple mutants (Fig. 4C). This model also provides an explanation for the partial suppression of the heterochromatic overreplication phenotype of *atxr5 atxr6* by mutations affecting DNA methylation (*5*). H3.3 is known to replace H3.1 at transcribed genes in plants and animals (*7*–*9*, *11*, *15*, *16*). Because loss of DNA methylation leads to the transcriptional activation of normally silent loci (*27*), DNA methylation mutants (similar to *fas2* mutants) would replace H3.1 with H3.3 in heterochromatin. Accordingly, suppression of overreplication is strongest in the DNA methylation mutants that have the greatest effect on transcriptional reactivation (*5*). Taken together, our results suggest a model in which H3.1K27me0 is the stimulus for heterochromatic overreplication.

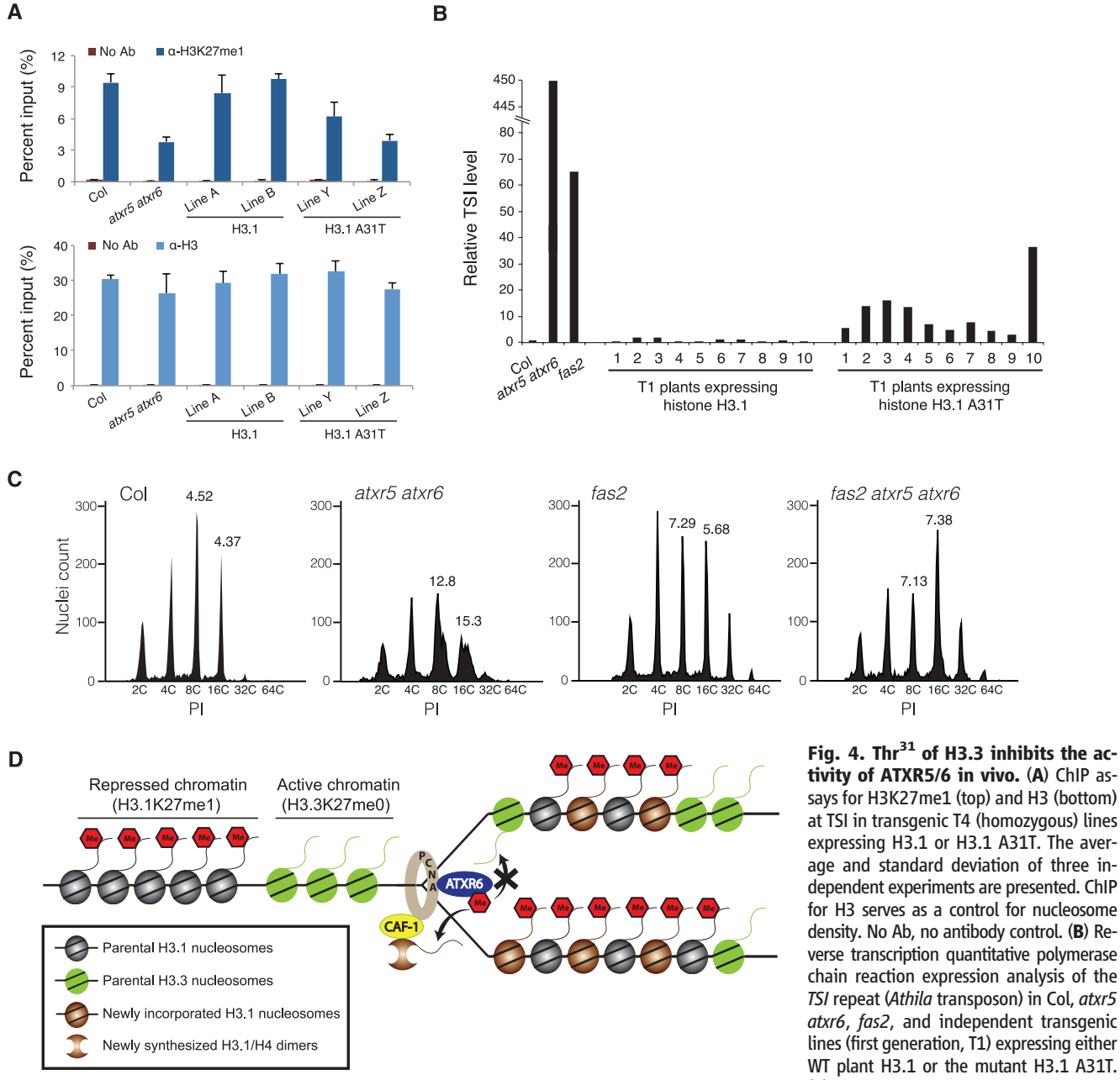

Fig. 4. Thr^{31} of H3.3 inhibits the activity of ATXR5/6 in vivo. (**A**) ChIP assays for H3K27me1 (top) and H3 (bottom) at TSI in transgenic T4 (homozygous) lines expressing H3.1 or H3.1 A31T. The average and standard deviation of three independent experiments are presented. ChIP for H3 serves as a control for nucleosome density. No Ab, no antibody control. (**B**) Reverse transcription quantitative polymerase chain reaction expression analysis of the *TSI* repeat (*Athila* transposon) in Col, *atxr5 atxr6*, *fas2*, and independent transgenic lines (first generation, T1) expressing either WT plant H3.1 or the mutant H3.1 A31T. (**C**) Flow cytometry profiles of Col, *atxr5 atxr6*, *fas2*, and *fas2 atxr5 atxr6* leaf nuclei. The numbers below the peaks indicate the endoreduplication (ploidy) levels of the nuclei. The numbers above the 8C and 16C peaks correspond to the robust CV values [propidium iodide (PI) units that enclose the central 68% of nuclei] for those peaks. High robust CV values at 8C and 16C peaks characterize heterochromatic over-replication (*4*). (**D**) Model for the role of ATXR5/6 during DNA replication in plants. Me, methyl group.

Overall, this study demonstrates how histone variants can determine epigenetic states through direct modulation of chromatin-modifying enzyme activity. Further, the ability of ATXR5/6 to discriminate between the variants H3.3 and H3.1 provides a mechanism for the mitotic inheritance and genome-wide distribution of H3K27me1 in plants. According to this model, ATXR5/6 are recruited to the replication fork during S phase through their interaction with PROLIFERATING CELL NUCLEAR ANTIGEN (PCNA) (*2*), where they specifically monomethylate K27 at newly incorporated, CAF-1–dependent H3.1 to rapidly restore this epigenetic mark (Fig. 4D) and prevent overreplication. This model does not rule out the possibility that some H3.1 might escape DNA replication–coupled K27 monomethylation (fig. S5). The inability of ATXR5/6 to methylate H3.3 may contribute to the protection of transcriptionally active, H3.3-enriched regions against H3K27me1 and repression during DNA replication.

References and Notes

1. C. Alabert, A. Groth, *Nat. Rev. Mol. Cell Biol.* **13**, 153–167 (2012).
2. C. Raynaud *et al.*, *Plant J.* **47**, 395–407 (2006).
3. Y. Jacob *et al.*, *Nat. Struct. Mol. Biol.* **16**, 763–768 (2009).
4. Y. Jacob *et al.*, *Nature* **466**, 987–991 (2010).
5. H. Stroud *et al.*, *PLOS Genet.* **8**, e1002808 (2012).
6. S. Smith, B. Stillman, *Cell* **58**, 15–25 (1989).
7. H. Tagami, D. Ray-Gallet, G. Almouzni, Y. Nakatani, *Cell* **116**, 51–61 (2004).
8. B. E. Schwartz, K. Ahmad, *Genes Dev.* **19**, 804–814 (2005).
9. A. D. Goldberg *et al.*, *Cell* **140**, 678–691 (2010).
10. P. Drané, K. Ouararhni, A. Depaux, M. Shuaib, A. Hamiche, *Genes Dev.* **24**, 1253–1265 (2010).
11. K. Ahmad, S. Henikoff, *Mol. Cell* **9**, 1191–1200 (2002).
12. A. Loyola, G. Almouzni, *Trends Biochem. Sci.* **32**, 425–433 (2007).
13. S. Henikoff, K. Ahmad, *Annu. Rev. Cell Dev. Biol.* **21**, 133–153 (2005).
14. Y. Mito, J. G. Henikoff, S. Henikoff, *Nat. Genet.* **37**, 1090–1097 (2005).
15. H. Stroud *et al.*, *Proc. Natl. Acad. Sci. U.S.A.* **109**, 5370–5375 (2012).
16. H. Wollmann *et al.*, *PLOS Genet.* **8**, e1002658 (2012).
17. L. Johnson *et al.*, *Nucleic Acids Res.* **32**, 6511–6518 (2004).
18. N. Schönrock, V. Exner, A. Probst, W. Gruissem, L. Hennig, *J. Biol. Chem.* **281**, 9560–9568 (2006).
19. A. Kirik, A. Pecinka, E. Wendeler, B. Reiss, *Plant Cell* **18**, 2431–2442 (2006).
20. L. Hennig, P. Taranto, M. Walser, N. Schönrock, W. Gruissem, *Development* **130**, 2555–2565 (2003).
21. T. Ono *et al.*, *Genes Cells* **11**, 153–162 (2006).
22. S. Takeda *et al.*, *Genes Dev.* **18**, 782–793 (2004).
23. D. Ray-Gallet *et al.*, *Mol. Cell* **44**, 928–941 (2011).
24. M. Endo *et al.*, *EMBO J.* **25**, 5579–5590 (2006).
25. V. Exner, P. Taranto, N. Schönrock, W. Gruissem, L. Hennig, *Development* **133**, 4163–4172 (2006).
26. E. Ramirez-Parra, C. Gutierrez, *Plant Physiol.* **144**, 105–120 (2007).
27. M. Rigal, O. Mathieu, *Biochim. Biophys. Acta* **1809**, 452–458 (2011).

Acknowledgments: We thank J. Calarco for critically reading the manuscript and J. Goodrich, C. Kohler, S. E. Jacobsen, D. J. Patel, and T. Schalch for materials and advice. Y.J. was supported by a Louis-Berlinguet postdoctoral fellowship (Fonds Québécois de la Recherche en Santé/Génome Québec). P.V. is supported by fellowships from the Deutsche Akademie der Naturforscher Leopoldina (LPDS 2009-5) and the Empire State Training Program in Stem Cell Research (NYSTEM, contract no. C026880). Work in the Reinberg laboratory is supported by grants from the NIH (GM064844 and R37GM037120) and the Howard Hughes Medical Institute. S.D.M. is supported by a grant from the NIH (GM075060). J.F.C. is supported by grants from the Canadian Institute of Health Research (BMA-355900) and the Natural Sciences and Engineering Research Council of Canada (Discovery Grant 191666) and acknowledges an Ontario Early Research Award and a Canada Research Chair in Structural Biology and Epigenetics. This work was supported by the Howard Hughes Medical Institute–Gordon and Betty Moore Foundation and by grants from the NSF (DBI-1025830) and the NIH (GM067014) to R.A.M. R.A.M. acknowledges a Chaire Blaise Pascal (Region Ile-de-France) at IBENS, Paris. The Protein Data Bank (PDB) accession number for the RcATXR5-H3.1-AdoHcy ternary structure is 4O30.pdb.

Supplementary Materials

www.sciencemag.org/content/343/6176/1249/suppl/DC1
Materials and Methods
Supplementary Text
Figs. S1 to S12
Table S1
References (*28*–*40*)

11 November 2013; accepted 12 February 2014
10.1126/science.1248357

Vertebrate Limb Bud Formation Is Initiated by Localized Epithelial-to-Mesenchymal Transition

Jerome Gros* and Clifford J. Tabin†

Vertebrate limbs first emerge as small buds at specific locations along the trunk. Although a fair amount is known about the molecular regulation of limb initiation and outgrowth, the cellular events underlying these processes have remained less clear. We show that the mesenchymal limb progenitors arise through localized epithelial-to-mesenchymal transition (EMT) of the coelomic epithelium specifically within the presumptive limb fields. This EMT is regulated at least in part by *Tbx5* and *Fgf10*, two genes known to control limb initiation. This work shows that limb buds initiate earlier than previously thought, as a result of localized EMT rather than differential proliferation rates.

In 1971, Searls and Janners found that, at early limb stages (Hamburger-Hamilton stage 17 to 18 in the chick), there is a substantial decrease in proliferation of the flank mesoderm, whereas higher rates are maintained within the emerging vertebrate limb buds. Accordingly, they proposed that localized regulation of proliferation at specific levels along the body axis is responsible for limb initiation (*1*). However, the cellular properties of the somatopleural lateral plate cells that give rise to the limb bud have not been identified.

During gastrulation, the mesodermal germ layer is formed through the generation of mesenchymal cells from the epithelial epiblast. However, shortly after gastrulation a reepithelization occurs such that essentially the entire embryo is epithelial, as defined by apical (F-actin) and basal (laminin) epithelial markers: Not only are the ectoderm, neural tube, and endoderm epithelial, but also the notochord, the somites, the intermediate mesoderm and the lateral plate mesoderm (i.e., splanchnopleural and somatopleural mesoderm, Fig. 1, A and D). At stage 13 in the chick, before any signs of limb bud formation, the somatopleure displays epithelial rather than mesenchymal characteristics. Molecular characterization revealed that, at this stage, F-actin and N-cadherin, as well as β-catenin and atypical protein kinase C (aPKC), localize at the apical end of somatopleure cells (Fig. 1, A and D, and fig. S1, A and D). On the other hand, vimentin is localized at the basal end of somatopleural cells, and laminin is deposited only on the basal side (Fig. 1, A and D, and fig. S1A), demonstrating that at early stages the somatopleure is a single cell layer and highly polarized, pseudostratified columnar epithelium. These observations differ from the previous assumption that limbs originate from a preexisting mesenchymal population. Forelimb bud mesenchyme first becomes apparent at stage 14 to 15, whereas the more posterior hindlimb mesenchyme can be first observed only at stage 15 to 16, as revealed by enrichment of vimentin expression and a concomitant loss of polarized localization of N-cadherin, β-catenin, F-actin, and aPKC within somatopleural cells and basement membrane of laminin breakdown (Fig. 1, B and E, and fig. S1, B, C, E, and F). Furthermore, mesenchyme in the trunk region is only seen at stage 17, long after forelimb and hindlimb mesenchymes have emerged (Fig. 1, C and F, and fig. S2), and thus out of order relative to the general rostral-caudal wave of development

Department of Genetics, Harvard Medical School, 77 Avenue Louis Pasteur, Boston, MA 02115, USA.

*Present address: Department of Developmental and Stem Cell Biology, Institut Pasteur, 25, 28 rue du Docteur Roux, 75724 Paris, Cedex 15, France.

†Corresponding author. E-mail: tabin@genetics.med.harvard.edu